Biodegradable and Biocompatible Nanocomposites of Poly(ϵ-caprolactone) with Hydroxyapatite Nanocrystals: Thermal and Mechanical Properties

Jianyuan Hao, Minglong Yuan, Xianmo Deng

Chengdu Institute of Organic Chemistry, Academia Sinica, P. O. Box 415, Chengdu 610041, People's Republic of China

Received 2 March 2001; accepted November 28, 2001

ABSTRACT: Nanocomposites of poly(ϵ-caprolactone) (PCL) with hydroxyapatite nanocrystals (HAP) prepared through the solvent-cast technique were characterized by means of transmission electron microscopy (TEM), differential scanning calorimetry (DSC), scanning electron microscopy (SEM), and tensile tests. Such composites are of great importance to make bone-like substitutes as HAP nanocrystals have similar composition, morphology, and crystal structure as natural apatite crystals. The TEM micrograph reveals the nanocrystals dispersed homogeneously in the matrix at a microscale level. The solvent-cast samples commonly show much higher melting points and crystallinity than the melt-quenched samples, due to a lower undercooling as well as more sufficient time to crystallize. For both cases of samples, the melting point decreases slightly with HAP content while the level of crystallinity attained by the PCL component is not hindered by the nanocrystals. Both the glass transition temperatures and the nonisothermal crystallization temperatures are composition dependent. The tensile modulus increases with increasing HAP content while the yield stress is almost invariant with composition. Theoretical prediction of the modulus based on Halpin–Tsai equations shows excellent agreement with the experimental result. By analysis of the variation in fracture stress and strain with composition, a ductile-to-quasi-brittle transition is revealed to be operative for the nanocomposites, as also can be seen by SEM. © 2002 Wiley Periodicals, Inc. J Appl Polym Sci 86: 676–683, 2002

Key words: biodegradable; biocompatable; nanocomposites

INTRODUCTION

The formation of inorganic–organic composites may produce materials that possess improved, comprehensive properties relative to individual components. Hydroxyapatite (HAP) has been used as a bone implant material in either sintered block or granular forms due to its excellent osteoconductivity as well as compatibility.[1,2] However, these application forms have some limitations regarding their mechanical and degradation properties. Sintered pure HAP could not degrade and thus may exist as foreign matter in the human body. Further, the high failure rate for pure HAP ceramics also impedes its clinical use. Thus in recent years, many studies on HAP focus on its composites with organic polymers especially those possessing biodegradability.[3–10] The polymeric parts are metabolized and excreted, and the ceramic constituents are assimilated in the body. The brittleness of HAP ceramics is also improved by mixing with tough organic polymers. Nevertheless, in these composites HAP commonly takes the form of polygonal sintered coarse particles, which has little similarity to natural bone apatite with regard to both particle morphology and size.

Recently a few reports have been presented concerning synthesis of HAP nanocrystals through the hydrothermal method.[11,12] In mature bone HAP nanocrystals are all irregular-shaped thin plates of carbonate apatite with average lengths and widths of 50×25 nm and thicknesses of 2–3 nm.[13–15]

Compared with sintered HAP particles, the hydrothermally formed needle-like nanocrystals have much more similarity in both morphology and crystal structure to those of natural apatite. Thus from the view of biomemetics, the nanocomposites containing HAP nanocrystals may achieve better osteoconductivity than those with sintered particles.[16–18] In addition to this physiological concern, making such nanocomposites also has mechanical consideration. Due to the submicron size and consequently huge specific surface area for HAP nanocrystals, the nanocomposites are expected to possess improved mechanical properties as compared with the pure polymer.

Liu has reported mechanical and physicochemical characteristics of nano-HAP/Polyactive 70:30 composites produced by the coprecipitation method.[19] The existence of HAP nanocrystals showed a strong ability to promote the calcification of the composites compared with the pure polymer. However, the initial

Correspondence to: J. Hao (jianyuan.hao@nottingham.ac.uk).

Journal of Applied Polymer Science, Vol. 86, 676–683 (2002)

mechanical strength for the composites is decreased by the nanocrystals, possibly due to their agglomeration. Previously, we have also successfully prepared poly(*d*,*l*-lactide) (PLA)/HAP nanocomposites through the solvent-cast technique.[20] The transmission electron microscopy (TEM) micrograph showed that HAP nanocrystals formed homogeneous dispersion in the PLA matrix at a microscopic level. This good dispersion for the nanocrystals resulted in the preservation of initial strength for the nanocomposites. Additionally, our ongoing degradation tests further demonstrate that in the buffer medium, the PLA/HAP nanocomposite films still preserve roughness and strength at the degradation stage of 4 months, which is in sharp contrast to the total lost of strength for pure PLA film. Such improvement in mechanical strength after degradation for a certain time may be ascribed to the calcification process of the nanocomposites.

Poly (ϵ-caprolactone) (PCL) is a biocompatible and biodegradable aliphatic polyester well known for a valuable set of properties such as nontoxicity for living organisms, resorption after an appropriate period of implantation time, and good ultimate mechanical properties.[21] Similar to PLA, PCL releases nontoxic by-products upon hydrolytic in vivo degradation.[22] A combination of PCL with HAP nanocrystals may produce flexible, rough bone implant materials in contrast to the rigidity of PLA/HAP nanocomposites. In this article, our research mainly focuses on thermal and mechanical properties of PCL/HAP nanocomposites.

EXPERIMENTAL

Preparation of HAP nanocrystals

HAP nanocrystals were synthesized by a hydrothermal method described elsewhere.[12,13] A $(NH_4)_2HPO_4$ aqueous solution of 200 mL (11.4 wt %) was slowly dropped into a stirred 400 mL $Ca(NO_3)_2$ aqueous solution (16.8 wt %). The pH for both solutions was 10–12, adjusted with ammonium hydroxide solution, and the reaction was carried out at room temperature. The resultant precipitates were put into an autoclave in a solid–solution ratio of 2 wt % and hydrothermally treated at 140°C and 0.3 MPa for 5 h, followed by centrifugal washing with deionized water. The hydrothermal slurry was finally dried and a white powder was obtained.

Synthesis of high molecular PCL

PCL was synthesized in bulk using 2-methylphenyl samarium as the initiator.[23] To describe the procedure briefly: ϵ-CL/initiator (1200/L) were added to a flask previously flamed, purged with nitrogen, and kept at 170°C for 30 min. The resulting polymer was then dissolved in $CHCL_3$, and recovered by precipitation in excess diethyl ether. The purified product was dried under vacuum at 40°C for 48 h. The M_w of the resulting polymer was 18.3×10^4 determined by intrinsic viscosity measurement using the relation $[\eta] = 9.94 \times 10^{-5} M_w^{0.82}$ in benzene at 30°C.

Dispersion of HAP nanocrystals in dimethylformamide (DMF)

Approximately 2 g of HAP nanocrystals was dispersed in 200 mL DMF using ultrasonics for 30 min. The dispersion was then filtered for removal of large aggregates and a blue sol filtrate was obtained. The accurate concentration of the sol was determined by precipitation of 10 mL of the sol into an excess of ethyl ether, followed by weighing the precipitate.

Preparation of PCL/HAP nanocomposites

PCL/HAP nanocomposites were prepared through a solvent-cast technique. Preweighed PCL was added into a flat-bottom flask that contained the HAP sol. The flask was sealed off and stirred at room temperature until PCL totally dissolved into the sol. The resulting mixture was poured into an aluminum mold and then heated to 140°C for 1 h in a thermostat oven for removal of the solvent. The nanocomposite film was furthered dried under vacuum at 80°C for 12 h.

Transmission electron microscopy

TEM was used to evaluate the dispersion of HAP nanocrystals in the PCL polymer matrix. The microscopic investigation was performed on a JEOL JEM-100CX TEM operating at 100 kV. The nanocomposite block was obtained from several pieces of composite films that were overlapped, and then treated under pressure at 140°C to melt into a thick pellet. The pellet was cut to form a triangular block face (approximately 1×0.5 mm) for microtoming. An ultrathin section was microtomed from this face, at room temperature, using an ultramicrotome. A water-filled boat was attached to the knife, so that after cutting, the ultrathin section could be floated onto water. The section was collected on a gold TEM grid and observed after drying in air.

Differential scanning calorimetry (DSC)

DSC analysis was performed to study thermal properties of the nanocomposites. The films obtained by casting were heated from −100 to 100°C. The melting temperatures (T_m) and apparent enthalpies of fusion (ΔH_f) were determined from DSC endothermic peaks. After being kept for 1 min at 100°C, the samples were cooled to −100°C and the crystallization exotherms were registered. From these cooling curves it was

possible to derive the nonisothermal crystallization temperatures (T_c). Unless otherwise indicated, a scan rate of 10°C min^{-1} was used throughout.

In order to detect the glass transition temperatures (T_g), additional DSC measurements were performed on melt-quenched samples. The melt-quenched samples were prepared by heating the solvent-cast nanocomposites to 100°C, held there for a min, and rapidly quenched to −100°C at a nominal rate of 40°C min^{-1}. The samples were then heated to 100°C at a rate of 10°C min^{-1}. The glass transition temperatures (T_g) were determined and the melting temperatures (T_m) and apparent enthalpies of fusion (ΔH_f) for melt-quenched samples were also recorded.

A DuPont 2100 was used throughout for all measurements under a nitrogen atmosphere.

Tensile tests

The stress–strain curves of solution-cast films were obtained at 15 °C on an Instron 4302 machine. The films were 0.1 mm thick and tested at a stretching speed of 50 mm/min. At least five specimens were measured and the mechanical tensile data were determined from the curves on the arithmetic average of three effectively broken specimens.

Scanning electron microscopy (SEM)

SEM was performed with an AMRAY 1000B equipment operated at 18 kV to examine the fracture surfaces of the nanocomposite films. The neck region for the broken specimens fractured in liquid nitrogen parallel to the draw direction in order to reveal the internal morphology. Prior to observation, the fracture surfaces were coated with a thin layer of gold by means of a polaron sputtering apparatus.

RESULTS AND DISCUSSION

Preparation of PCL/HAP nanocomposites

HAP nanocrystals were prepared through precipitation reaction followed by hydrothermal treatment of the resultant slurry, as described in the experimental part. The hydrothermally formed nanocrystals are rod-like particles with the length between 40 and 80 nm, and width between 20 and 40 nm. The Ca/P ratio and the surface area of these nanocrystals were determined as 1.61 by an atomic absorption spectrometer for calcium combined with an ultraviolet spectrophotometer for phosphorus, and 80 m^2/g by the Brunauer–Emmett–Teller (BET) method, respectively. Compared with sintered HAP particles, the hydrothermally formed nanocrystals have much more similarity in morphology, crystal structure, composition, and crystallinity as those of natural apatite.

TABLE I
Sample Preparation and Designations for PCL/HAP Nanocomposites

Sample code	PCL (g)	HAP sol (mL)	HAP content (wt %)
PCL/HAP (0)	1.00	0	0
PCL/HAP (7.4%)	1.00	12.0	7.4
PCL/HAP (13.8%)	1.00	24.0	13.8
PCL/HAP (19.4%)	1.00	36.0	19.4
PCL/HAP (24.2%)	1.00	48.0	24.2
PCL/HAP (28.6%)	1.00	60.0	28.6

However, application of HAP nanocrystals has been impeded for making organic–inorganic nanocomposites due to their easy agglomeration when separated from the aqueous medium. Liu has previously reported preparation of nano-HAP/Polyactive 70:30 composites by coprecipitation of the suspension mixture of the polymer chloroform solution with suspended HAP nancorystals.[19] The decreased mechanical strength with HAP content implied a certain agglomeration of the nanocrystals in the matrix. Our recent study shows that HAP nanocrystals may form nanoscale dispersion in the DMF solvent. The resultant gel is a blue, stable suspension that could be preserved for several days with only slight precipitation. This feature offers possibility to prepare real polymer/HAP nanocomposites through the solvent-cast technique.

The details for preparation of PCL/HAP nanocomposites are shown in the experimental part. The accurate concentration of the sol containing HAP particles was determined as 100 mg/15 mL by precipitating it into an excess of ethyl ether, followed by weighing the precipitate. The content of HAP in the nanocomposite could be easily adjusted by varying the feed ratio for PCL weight/HAP-sol volume. Sample preparation and designations for PCL/HAP nanocomposites are listed in Table I.

Figure 1 shows the dispersion of HAP nanocrystals in the PCL polymer matrix. It is shown that homogeneous distribution of the nanocrystals at a microscopic level is observed in the matrix. So far this dispersion level is the best working result for polymer/HAP composites.

Thermal properties of PCL/HAP nanocomposites

Schemes of thermal analysis described before were conducted to study the thermal properties of PCL/HAP nanocomposites. The melting temperature of PCL is greatly decided by both the HAP content in the nanocomposite as well as the sample's thermal history. Figure 2 shows the variations of melting temperature as a function of HAP content for both solvent-cast and melt-quenched samples. A slight decrease in

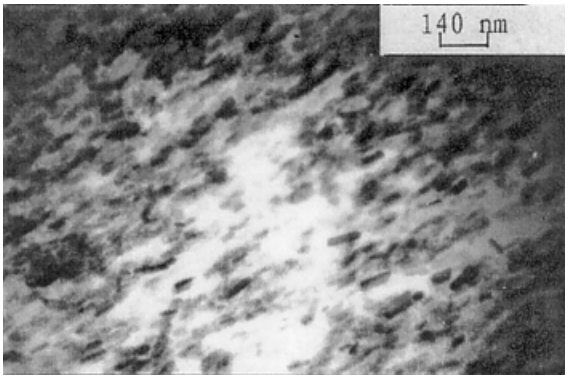

Figure 1 Dispersion of HAP nanocrystals in the PCL/HAP (28.6%) nanocomposite.

melting point with composition is observed for the solvent-cast samples. Generally, a sample with a higher melting point means the produced crystals are more perfect—namely, much thicker or having higher degree of order. Thus the above result indicates that under the present preparation conditions, the presence of HAP nanocrystals may decrease the degree in perfection of PCL crystals in the solvent-cast samples. This influence may be ascribed to additional energy requirement for expulsion of HAP nanocrystals from surfaces of PCL as-formed crystals, and then impeding their thickening. Also due to the same reason, a similar decrease in melting point with composition has also been observed in the case of melt-quenched samples.

Compared with the effect of the nanocrystals, thermal history affects much more on melting point. From Figure 2, the solvent-cast samples commonly show much higher melting points than the melt-quenched samples. For the solvent-cast samples, they were slowly cooled in a vacuum oven from the temperature

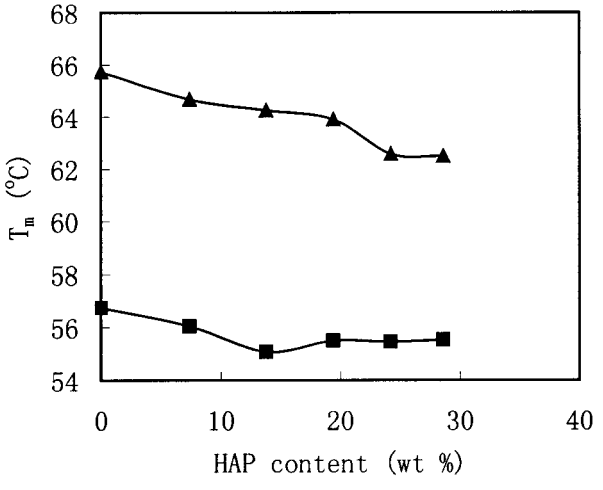

Figure 2 Variations of melting temperature of PCL (T_m) as a function of HAP content: solvent-cast samples (▲); melt-quenched samples (■).

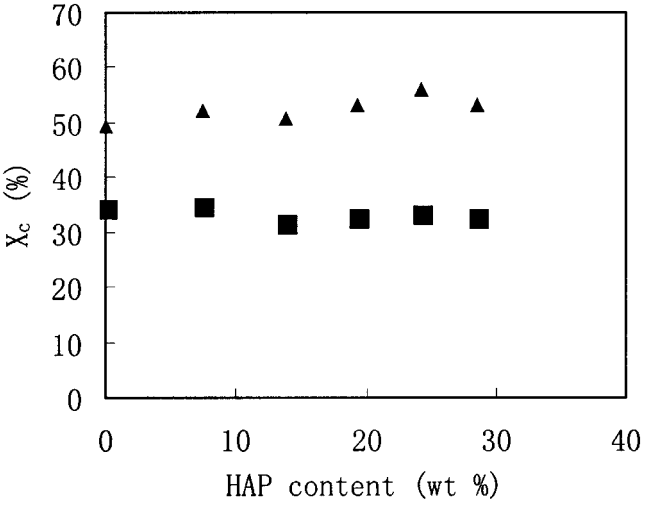

Figure 3 Variations of crystallinity of PCL (X_c) as a function of HAP content: solvent-cast samples (▲); melt-crystallized samples (■).

of 80°C to room temperature (roughly at a rate of 0.2°C min^{-1}), which is in sharp contrast to a rapid cooling rate (40°C min^{-1}) for melt-quenched samples. This quenching effect results in a larger undercooling for the crystallization of the melt-quenched samples, thus producing their much lower melting points than the solvent-cast samples.

From Figure 2, it has also been observed that the melt-quenched samples show a more slight decrease in melting point with composition relative to the solvent-cast samples. This is also due to the quenching effect that partially offsets the effect of HAP nanocrystals on melting points of the nanocomposites.

The crystallinity, X_c, of the PCL component in the nanocomposite is obtained according to the following relation:

$$X_c = \Delta H_f / (w \times \Delta H_{f,100\%}) \quad (1)$$

where $\Delta H_{f,100\%}$ and ΔH_f indicate the heats of fusion for a 100% crystalline PCL and the nanocomposite, respectively, w is the weight fraction of PCL in the nanocomposite, the value of $\Delta H_{f,100\%}$ is taken as 142 J g^{-1} for calculation.[24] The variations of crystallinity with composition for both solvent-cast and melt-quenched samples are illustrated in Figure 3. Quite remarkable is that the quenching process for melt-quenched samples could effectively decreased the crystallinity of the PCL component, as compared with those for solvent-cast samples. Further, it is also seen that both types of samples show a constant level of crystallinity for all the compositions investigated. This indicates that for both cases of samples, the difference in crystallization kinetics resulting from different HAP content is insufficient to induce a change in crystallinity of the PCL component.

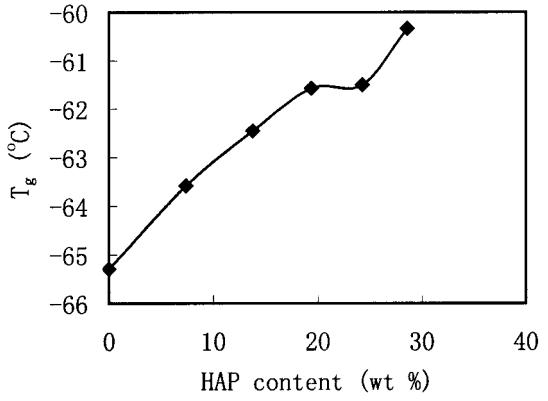

Figure 4 Variation of glass transition temperature of PCL (T_g) as a function of HAP content.

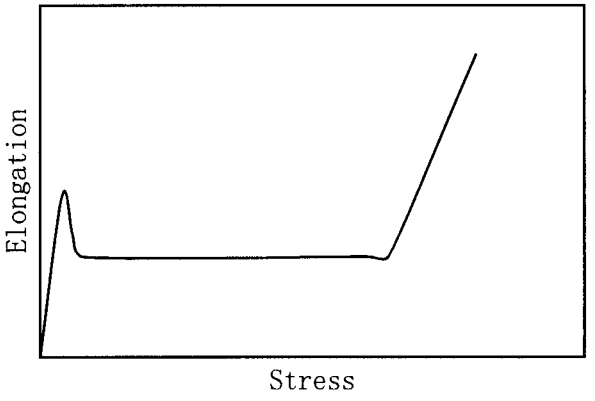

Figure 6 Schematic stress–strain curve for the nanocomposites.

The solvent-cast samples show no sign of glass transitions on their DSC heating curves. This is despite the fact that the amorphous part roughly proportions 50% of the PCL component. It is thus deduced that the phase separation for amorphous and crystalline parts of the PCL component must occur on a very small scale. In order to examine the influence of HAP content on glass transition temperature of the PCL component, DSC heating experiments were performed on melt-quenched samples and the results are shown in Figure 4. As a rule, the T_g value of PCL would increase with increasing HAP content. Actually, T_g is observed to increase from −65.29°C for pure PCL to 60.33°C for the nanocomposite containing 28.6 wt %.

Nonisothermal crystallization for the nanocomposites was studied by cooling the melt samples from 100 to −100°C at a rate of 10°C min^{-1}. The variation of nonisothermal crystallization temperature with HAP content is illustrated in Figure 5. It is seen that the nanocomposites all show higher T_c values than the pure polymer. This is a reflection of the effect of HAP nanocrystals on crystallization kinetics of the PCL component. Commonly, the kinetic for nonisothermal crystallization is governed by two factors—namely, the nucleation as well as the growth rates. Whereas the presence of HAP crystals may decrease the growth rate, their existence could also accelerate the nucleation of the PCL segments. Thus if the latter effect prevails over the former, the total crystallization rate for the nanocomposites is increased. Such is actually shown by a shift of T_c to higher temperature when compared with that for pure PCL.

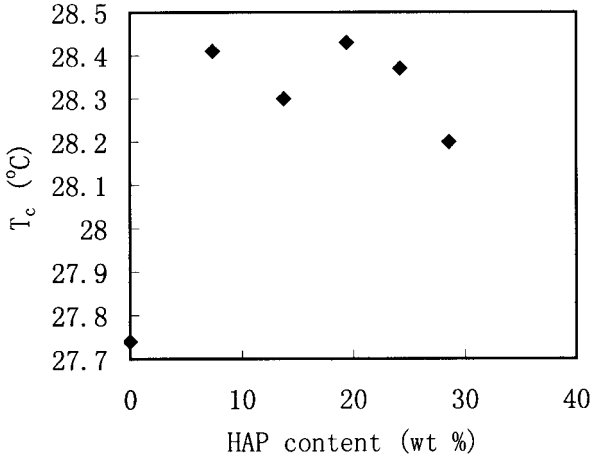

Figure 5 Variation of nonisothermal crystallization temperature of PCL (T_c) as a function of HAP content.

Mechanical properties of PCL/HAP nanocomposites

Figure 6 shows the schematic stress–strain curve for the nanocomposites. The specific character of an actual curve is intimately linked with the HAP content in the nanocomposites. In the case of pure PCL, the stress–strain curve is typical of ductile, semicrystalline polymers. That is, the sample initially proceeds with elastic deformation and after reaching the yield point, the stress drops to a constant value and maintains this level until the strain reaches about 800%. Beyond this point, with further increased strain, the stress rapidly increases until attaining to the fracture strain of 1420%. Similar curves have also been observed for the nanocomposites with HAP content below 24.2 wt %. All samples undergo the final strain-hardening period despite the fracture stress and strain varied with composition. However for the PCL/HAP (28.6%) nanocomposite that contains the highest HAP content, the sample breaks after its yield but prior to the strain-hardening period.

Figure 7 shows the dependence of tensile modulus on HAP content for the nanocomposites. The presence of the filled nanocrystals substantially increases the tensile modulus relative to the pure polymer. For the nanocomposite containing 28.6 wt % HAP, the modulus even reaches to 501.8 MPa as compared to 294 MPa for pure PCL. The increase in modulus with filler

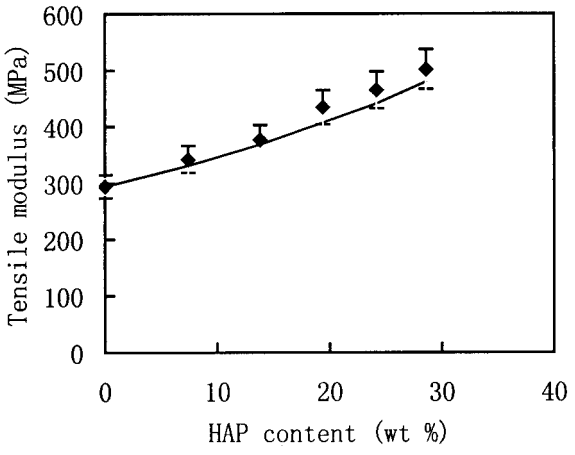

Figure 7 Dependence of tensile modulus on HAP content; the solid line was calculated from eq. (5).

content could be theoretically predicted by assuming the nanocomposite as a short fiber-filled system. For a composite containing unidirectional arrayed fibers, the effect of filler on moduli could be described using Halpin–Tsai equations[25]:

$$E_L = \frac{1 - K_L V_f}{1 + 2(l_f/d_f)K_L V_f} E_m \tag{2}$$

$$E_T = \frac{1 + 2K_T V_f}{1 - K_T V_f} E_m \tag{3}$$

with

$$K_L = \frac{(E_f/E_m) - 1}{(E_f/E_m) + 2(l_f/d_f)} \tag{4}$$

$$K_T = \frac{(E_f/E_m) - 1}{(E_f/E_m) + 2} \tag{5}$$

where E_L and E_T are the composite moduli in the longitudinal and transverse direction of the fibers orientation, respectively; E_m and E_f are the matrix and the filler moduli, respectively; V_f is the volume fraction of the filler; l_f is the average length of the filler; d_f is the average thickness of the filler. However, for the cases of PCL/HAP nanocomposites, the spatial orientation of the nanocrystals is not a one-dimensional alignment but a random array in three dimensions. For such a composite, the modulus could be estimated from below experimental equation on the basis of eqs. (1) and (2)[26]:

$$E_r = \frac{3}{8}E_L + \frac{5}{8}E_T \tag{6}$$

The solid line in Figure 7 is the prediction of the modulus obtained from eq. (6). For our calculations, the moduli of the PCL matrix (E_m) and the HAP nanocrystals (E_f) are taken as 114.0 and 0.294 GPa, respectively[27]; the value of l_f/d_f for the nanocrystals is taken as 3; the densities for the PCL and HAP components are taken as 1.146 and 3.219 g cm^3, respectively.[28,29] It is seen that the experimental values fall on the solid line, indicating the good agreement between prediction and experiment.

Figure 8 illustrates the dependence of yield stress and fracture stress on HAP content, respectively. It is observed that the yield stress for the nanocomposites varies little with HAP content. In a first approximation, the yield stress is almost unaffected by HAP content. This result is simply a reflection of the fact that good adhesion between the matrix and the filler is maintained for the nanocomposites prior to their occurrence of yield. That the yield stress has been decreased by the nanocrystals also indicates their good dispersion in the polymer matrix. Actually, if the nanocrystals are not well dispersed in the matrix but agglomerate heavily, the internal crack of the aggregate particles would make them no longer bear load, thus resulting in a decreased stress for the nanocomposites. The preservation of yield stress with HAP content shows no clear sign of reinforcing effect of the nanocrystals on the polymer matrix. Kelly and Tyson have suggested a plastic stress transfer model to predict the values of stress for short-fiber reinforced systems.[30] According to their theory, above result could be ascribed to two factors—namely, as lower matrix-fiber interfacial shear stress as well as lower aspect ratio for the nanocrystals.

From Figure 8, the fracture stress decreases with HAP content due to the nanocrystals gradually debonding from the matrix after the neck formation. This has been evidenced by the appearance of profuse whitening of the samples accompanying with formation and propagation of the neck. Thus the load ap-

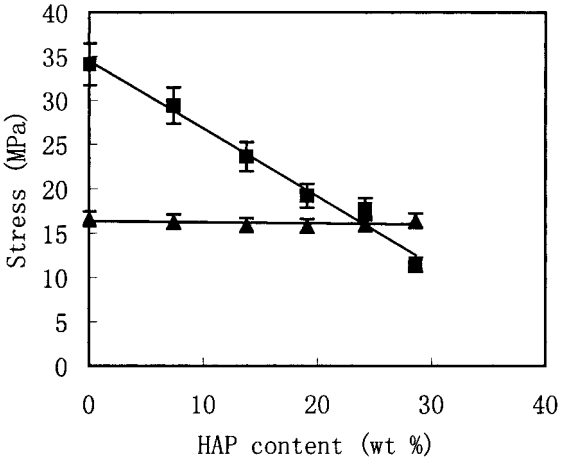

Figure 8 Dependence of yield stress (▲) and fracture stress (■) on HAP content.

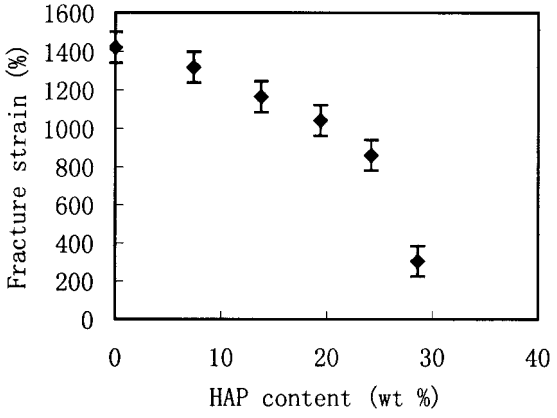

Figure 9 Dependence of fracture strain on HAP content.

plied to the samples is only carried by the polymer itself. According to this model, there is a critical composition at which the fracture stress drops to the value of draw stress. For our cases, the draw stress is roughly about 11.4 MPa and the critical composition is between 24.2 and 28.6 wt %. Below this composition, the fracture stress linearly decreases with increasing HAP content.

The dependence of fracture strain with HAP content is shown in Figure 9. Below the critical composition, the samples undergo the strain-hardening period and the PCL polymer in the samples is regarded as attaining its maximum strain (fracture strain) prior to their fracture. Thus the fracture strain for the nanocomposites only decreases slightly with composition, as shown in Figure 9. However, when the composition surpasses the critical value, the draw stress exceeds the strength of the strain-hardening PCL ligaments in the cross section. Then the samples break at the point where PCL ligaments have not reached the maximum strain. This leads to a sharp decrease of the fracture stain for the case of PCL/HAP nanocomposite (28.6 wt %). This transition of fracture strain for the nanocomposites is generally called a ductile-to-quasi-brittle transition. Figure 10 shows the fracture surfaces of pure PCL and the PCL/HAP (28.6%) nanocomposite, respectively. The observed surfaces were acquired by fracture the neck regions of the broken samples parallel to the draw direction in liquid nitrogen. In the case of pure polymer, it is seen that obvious PCL ligaments, parallel to each other, are aligned along the draw direction due to adequate deformation. This is in sharp contrast to relatively smooth surface for the PCL/HAP (28.6%) nanocomposite, which indicates a quasi-brittle fracture mode of the sample.

SUMMARY AND CONCLUSIONS

In this article nanocomposites of PCL/HAP were prepared by the solvent-cast technique. Such composites are of great importance for making bone-like substitutes as HAP nanocrystals have similar composition, morphology, and crystal structure as those of natural apatite crystals. The dispersion of HAP nanocrystals in the polymer matrix is homogeneous at a microscopic level, as revealed by TEM.

The thermal properties of PCL/HAP nanocomposites were investigated by DSC for solvent-cast and melt-quenched samples. The solvent-cast samples commonly show much higher melting points and crystallinity than the melt-quenched samples, due to a lower undercooling as well as more sufficient time to crystallize. For both cases of samples, the melting point increases with increasing HAP content while the level of crystallinity attained by the PCL component is not hindered by the nanocrystals. The glass transition temperatures obtained from the melt-quenched samples show an increase with increasing HAP content. The nonisothermal crystallization temperatures for the nanocomposites show higher values than the pure polymer. This indicates that the presence of HAP nanocrystals may accelerate the nucleation of the PCL segments.

The tensile modulus for the nanocomposites increases with increasing HAP content. Theoretical prediction of the modulus has been made by assuming the nanocomposite as a short fiber-filled system. The

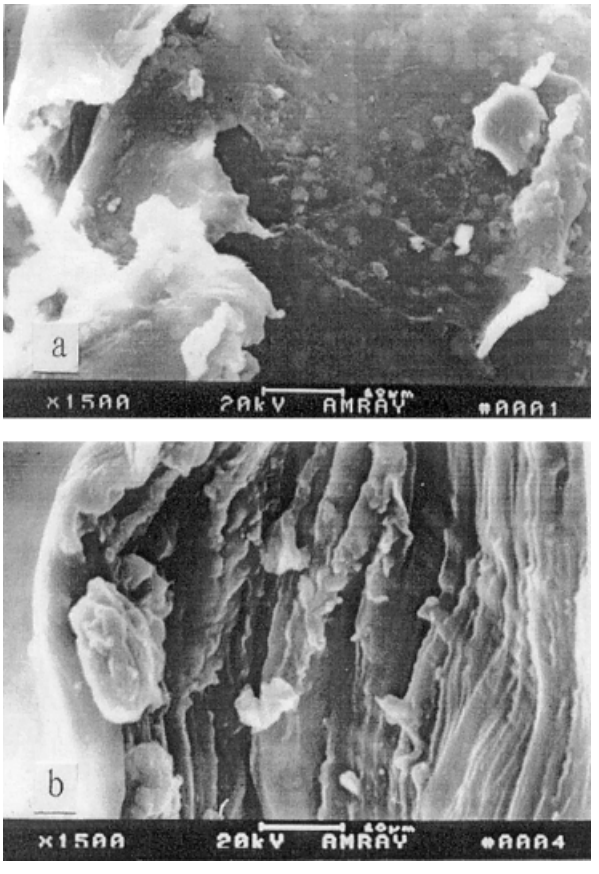

Figure 10 Fracture surfaces of pure PCL (b) and the PCL/HAP (28.6 wt %) nanocomposite (a).

calculation values based on Halpin–Tsai equations show excellent agreement with the experimental results. The yield stress has not been undermined by the presence of the nanocrystals. This preservation of strength for the nanocomposites may be due to the homogeneous dispersion of the nanocrystals in the PCL matrix. By analysis of the variation in fracture stress and strain with composition, a ductile-to-quasi-brittle fracture transition is revealed to be operative for the nanocomposites. Such a transition occurs between the composition of 24.2 and 28.6 wt %, and is also revealed by SEM.

References

1. Makishima, A.; Aoki, H. In Bioceramics; Yamaguchi, T., Yanagida, H., Eds.; Gihodo: Tokyo, 1984; p 6.
2. Daculsi, G.; Passuti, N. In Bioceramics II, Onishi, H., Hemeke, E., Eds.; Ishigakuro: Tokyo, 199; p 345.
3. Liu, Q.; de Wijn, J. R.; Bakker, D.; Van Blitterswijk, C. A. J Mater Sci, Mater Med 1996, 7, 551.
4. Kikuchi, M.; Suetsugu, Y.; Tanaka, J.; Akao, M. J Mater Sci, Mater Med 1997, 8, 361.
5. Verheyen, C. C. P. M.; Klein, C. P. A. T.; de Blieckhogervorst, J. M. A.; Wolke, J. G. C.; van Blitterswijn, C. A. J Mater Sci, Mater Med 1993, 4, 58.
6. Verheyen, C. C. P. M.; de Wijn, J. R.; van Blitterswijk, C. A.; de Groot, K. J Biomed Mater Res. 1992, 10, 1277.
7. Cerrai, P.; Guerra, G. D.; Tricoli, M.; et al. J Mater Sci, Mater Med 1999, 5, 283.
8. Jin, S.; Gonsalves, K. E. J Mater Sci, Mater Med 1999, 6, 363.
9. Shikinami, Y.; Okuno, M. Biomaterials 1999, 9, 859.
10. Ignjatovic, N.; Tomic, S.; Dakic, M.; et al. Biomaterials 1999, 9, 809.
11. Li, Y. B.; de Wijn, J.; Klein, C. P. A. T.; Van de Meer, S. J Mater Sci, Mater Med 1994, 5, 252.
12. Li, Y. B.; de Groot, K.; de Wijn, J.; Klein, C. P. A. T.; Van de Meer, S. J Mater Sci, Mater Med 1994, 5, 326.
13. Lowenstam, H. A.; Weiner, S. On Biomineralization; Oxford University Press: New York, 1989.
14. Robinson, R. A. J Bone Joint Surg 1952, 34A, 389.
15. Weiner, S.; Price, P. A. Calcif Tissue Int 1986, 39, 365.
16. Posner, A. S. Clin Orthop Rel Res 1985, 200, 87.
17. Ellies, L. G.; Garter, J. M.; Natiella, J. R.; Featherstone, J. D. B.; Nelson, D. G. A. J Biomed Mater Res 1988, 22, 137.
18. Li, Y.; Klein, G. P. A. T.; de Wijn, J.; van de Meer, S.; Groot, K., J. Mater. Sci., Mater. Med., 1994, 5, 263.
19. Liu, Q.; de Wijn, J.; van Blitterswijk, C. A. Biomaterials 1997, 18, 1263.
20. Deng, X. M.; Hao, J. Y.; Wang, C. S. Biomaterials 2001, 21, 2867.
21. Pitt, C. G.; Marks, T. A.; Schindler, A. In Controlled Release Bioactive Materials; Baker, R., Ed.;, Academic Press: New York, 1980.
22. Schindler, A.; Jeffcoat, R.; Kimmel, G. L.; Pitt, C. G.; Wall. M. E.; Zweidinger, R. In Contemporary Topics in Polymer Science, Vol. 2; Pearce, J. R., Schaefger, E. M., Eds., Plenum: New York, 1977; p 251.
23. Yuan, M. L.; Li, X. H.; Xiong, C. D.; Deng, X. M. Eur Polym J 1999, 35, 2131.
24. Wunderlich, B. In Macromolecular Physics, Vol. 3, Crystal Melting; New York: Academic Press, 1980; p 54.
25. Halpin, J. S.; Tsai, S. M. AFML-TR 67-423, June, 1969.
26. Mallick, P. K. Fiber-Reinforced Composites: Materials, Manufacturing, and Design; Marcel Dekker: New York, 1988; p 110.
27. Gilmore, R. S.; Katz, J. L. J Mater Sci 1982, 17, 1131.
28. Park, J. B.; Lakes, R. S. Biomaterials: An Introduction; Plenum Press: New York, 1992.
29. Glicher, S. J. Phil Trans R Soc Lond 1984, B304, 470.
30. Kelly, A.; Tyson, W. R. J Mech Phys Solids 1965, 13, 329.